The Astronomical Journal, 153:76 (6pp), 2017 February doi:10.3847/1538-3881/153/2/76

IMAGING OBSERVATIONS OF THE HYDROGEN COMA OF COMET 67P/CHURYUMOV–GERASIMENKO IN 2015 SEPTEMBER BY THE *PROCYON*/LAICA

Yoshiharu Shinnaka[1,2], Nicolas Fougere[3], Hideyo Kawakita[4], Shingo Kameda[5], Michael R. Combi[3], Shota Ikezawa[5], Ayana Seki[5], Masaki Kuwabara[6], Masaki Sato[5], Makoto Taguchi[5], and Ichiro Yoshikawa[6]
[1] National Astronomical Observatory of Japan, 2-21-1 Osawa, Mitaka, Tokyo 181-8588, Japan; yoshiharu.shinnaka@nao.ac.jp
[2] Institut d'Astrophysique et de Géophysique, Université de Liège, Allée du Six Août 17, B-4000 Liége, Belgium
[3] Department of Climate and Space Sciences and Engineering, University of Michigan, 2455 Hayward Street, Ann Arbor, MI 48109-2143, USA
[4] Laboratory of Infrared High-resolution spectroscopy (LiH), Koyama Astronomical Observatory, Kyoto Sangyo University, Motoyama, Kamigamo, Kita, Kyoto 603-8555, Japan
[5] Department of Physics, Rikkyo University, 3-34-1 Nishi-Ikebukuro, Toshima, Tokyo 171-8501, Japan
[6] Department of Complexity Science and Engineering, The University of Tokyo, 5-1-5 Kashiwanoha, Kashiwa, Chiba 277-8561, Japan
Received 2016 October 16; revised 2016 December 6; accepted 2016 December 6; published 2017 January 24

ABSTRACT

The water production rate of a comet is one of the fundamental parameters necessary to understand cometary activity when a comet approaches the Sun within 2.5 au, because water is the most abundant icy material in the cometary nucleus. Wide-field imaging observations of the hydrogen Lyα emission in comet 67P/Churyumov–Gerasimenko were performed by the Lyman Alpha Imaging Camera (LAICA) on board the 50 kg class micro spacecraft, the *Proximate Object Close Flyby with Optical Navigation* (*PROCYON*), on UT 2015 September 7.40, 12.37, and 13.17 (corresponding to 25.31, 30.28, and 31.08 days after the perihelion passage of the comet, respectively). We derive the water production rates, Q_{H_2O}, of the comet from Lyα images of the comet by using a 2D axi-symmetric Direct Simulation Monte-Carlo model of the atomic hydrogen coma; $(1.46 \pm 0.47) \times 10^{28}$, $(1.24 \pm 0.40) \times 10^{28}$, and $(1.30 \pm 0.42) \times 10^{28}$ molecules s^{-1} on 7.40, 12.37, and 13.17 September, respectively. These values are comparable to the values from in situ measurements by the *Rosetta* instruments in the 2015 apparition and the ground-based and space observations during the past apparitions. The comet did not show significant secular change in average water production rates just after the perihelion passage for the apparitions from 1982 to 2015. We emphasize that the measurements of absolute Q_{H_2O} based on the wide field of view (e.g., by the LAICA/*PROCYON*) are so important to judge the soundness of the coma models used to infer Q_{H_2O} based on in situ measurements by spacecraft, like the *Rosetta*.

Key words: comets: general – comets: individual (67P/Churyumov–Gerasimenko) – methods: observational

1. INTRODUCTION

Secular change and mass-loss rate of a comet are clues to understand the evolution of surface structures of the nucleus. Within ~2.5 au from the Sun, the water production rate of a comet is used to evaluate cometary (mass-loss) activity because water is the most abundant molecular species in the cometary nucleus (~70% of icy materials). As A'Hearn et al. (1995) pointed out, the slopes of the water production rate with respect to heliocentric distance, r_H, of comets seem to depend on dynamical ages of the comets. The dynamically older comets (especially, Jupiter-family comets) have steeper slopes of water production rates with respect to r_H (usually steeper than a canonical r_H^{-2} dependence) and therefore, the slopes of the water production rates are not primordial and the variation in the slopes may be evolutionary effects. However, we cannot rule out the possibility that the observed difference in slopes between dynamical new comets and short-period comets reflects the primordial properties of those comets (e.g., their formation regions in the solar nebula and compositions of icy materials).

Comet 67P/Churyumov–Gerasimenko (hereafter 67P/C–G) is a Jupiter-family comet with an orbital period of ~6.45 years. The Tisserand invariant with respect to Jupiter is 2.75, calculated from its orbital parameters listed in JPL's HORIZONS system.[7] During the 2015 apparition of the comet, its perihelion distance was 1.243 au at UT 2015 August 13.0908. This apparition of the comet was interesting because 67P/C–G was the target of ESA's *Rosetta* mission. The comet was probed by the *Rosetta* spacecraft close to the nucleus and by the Philae lander on the comet surface. Many interesting results for volatiles were already reported, such as the first detection of multiple complex organic molecules and the simplest form of amino acids, glycine, which could be key building blocks of life (Goesmann et al. 2015; Altwegg et al. 2016), and primordial molecular oxygen and nitrogen (Bieler et al. 2015a; Rubin et al. 2015). Water production rates of the comet have been also derived by various instruments on board the *Rosetta* spacecraft throughout the 2015 apparition (Biver et al. 2015; Bockelée-Morvan et al. 2015, 2016; Fougere et al. 2016a, 2016b; Hansen et al. 2016; Wedlund et al. 2016 and references therein). However, measurement of an absolute water production rate is difficult because the *Rosetta* spacecraft was located in the cometary coma. Note that an obtained water production rate strongly depends on the coma models, notably due to the asymmetry of the coma. To derive gas production rates based on in situ measurements by the *Rosetta* instruments, at the close distances from the comet 67P/C–G, the observations performed by the wide field of view (FOV) instruments from the ground-based and space observatories, like the Lyman Alpha Imaging Camera (LAICA) on board the Proximate Object Close Flyby with Optical Navigation (PROCYON), can realize the critical calibration for the gas production rates to be compared with those derived from in situ measurements.

[7] http://ssd.jpl.nasa.gov/horizons.cgi

Table 1
Observational Circumstances of 67P/C–G Taken with the *PROCYON*/LAICA and Derived Water Production Rates

UT Time on 2015	ΔT (days)	T_{exp} (s)	r_H (au)	Δ_s (au)	g (photons s^{-1} $atom^{-1}$)	Q (molecules s^{-1})	χ^2_{red}	S_A (m^2)	f_A (%)
Sep 7 9:31–9:47	25.305	300	1.282	1.841	8.34×10^{-4}	1.46×10^{27}	1.04	$(3.5 \pm 1.1) \times 10^6$	7.3 ± 2.4
Sep 12 8:58–9:01	30.281	200	1.298	1.836	8.13×10^{-4}	1.24×10^{27}	1.04	$(3.0 \pm 1.0) \times 10^6$	6.4 ± 2.0
Sep 13 4:00–4:15	31.076	600	1.301	1.835	8.09×10^{-4}	1.30×10^{27}	1.38	$(3.2 \pm 1.0) \times 10^6$	6.7 ± 2.2

Note. UT Time is the start and end for each observation. ΔT is days from perihelion passage (2015 August 13.08425) for each observation. T_{exp}. is total exposure time in seconds. r_H and Δ_s indicate heliocentric distance and distance between the *PROCYON* spacecraft and the 67P/C–G in au, respectively. g is a g-factor at the observations (photons s^{-1} $atom^{-1}$). Q is the best-fit water production rate (molecules s^{-1}). The 1σ error level of each Q is 32%, which includes both systematic error caused by the uncertainties of observing flux calibration of 30% and of g-factor of 10% and random error by the uncertainty of model fitting of 1%. χ^2_{red} is the best-fit reduced-χ^2 of each observation. S_A and f_A indicate the active areas (m^2) and active area fractions (%), and these are calculated by using the gas production rate per area at 1 au ($Z = 0.69 \times 10^{22}$ molecules s^{-1} m^{-2}; Keller 1990, pp. 13–68).

For comet 67P/C–G, the water production rates have been derived from OH observations in the near-ultraviolet wavelength region during the apparitions in 1982 and 1996 (A'Hearn et al. 1995; Crovisier et al. 2002; Feldman et al. 2004; Schleicher 2006), from low-resolution spectroscopic observations of water in the near-infrared wavelength region during the apparition in 2009 by the *AKARI* satellite (Ootsubo et al. 2012), and also from Lyα observations in the ultraviolet wavelength region by Solar Wind ANisotropies (SWAN) all-sky camera on board the *Solar and Heliospheric Observatory* (*SOHO*) satellite during the last three apparitions in 1996, 2002, and 2009 (Bertaux et al. 2014). Bertaux et al. (2014) demonstrated that the water production rates around perihelion were 1.3×10^{28}, 1.8×10^{28}, and 5.65×10^{27} molecules s^{-1} for apparitions in 1996, 2002, and 2009, respectively. Based on their results, the comet did not show significant secular change in average water production rates just after its perihelion passage. It was expected that 67P/C–G would show a similar level of activity around the perihelion passage (2015 August) based on the observations in the last three apparitions (Bertaux et al. 2014). In comparison with the observed slopes of water production rate in other comets, comet 67P/C–G showed relatively steeper slopes in the 1982 apparition (A'Hearn et al. 1995). In the 2015 apparition, a slight offset (a few weeks after perihelion) in the peak of water production rate was shown by the ROSINA and the VIRTIS instruments of the *Rosetta* spacecraft (Bockelée-Morvan et al. 2016; Fougere et al. 2016b; Hansen et al. 2016).

2. OBSERVATIONS AND DATA REDUCTION

On UT 2015 September 7.40, 12.37, and 13.17 (25.31, 30.28, and 31.08 days after the perihelion passage, respectively), we performed wide-field imaging observations of Lyα emission in comet 67P/C–G by the LAICA on board the first 50 kg class micro spacecraft for deep space exploration, the *PROCYON* (Funase et al. 2015). Observational circumstances at each observation are listed in Table 1.

The *PROCYON* spacecraft was launched on UT 2014 December 3 from the Tanegashima Space Center in Kagoshima, Japan on the H-IIA F-26 rocket. The primary mission of the *PROCYON* was the demonstration of a micro-spacecraft bus system for deep space exploration. The secondary (advanced) missions consist of engineering and scientific missions. The engineering mission includes the low-thrust deep space maneuver for performing an Earth swing-by and changing the trajectory to flyby a near-Earth asteroid and a high-resolution observation of a near-Earth asteroid during a close (<30 km) and fast (~10 km s^{-1}) flyby (Funase et al. 2015). The main purpose of scientific mission was the wide-view imaging observations of the whole geocorona and geotail from deep space using the LAICA telescope. Operation of the *PROCYON* was already finished in 2015 December.

The LAICA is a spherical Cassegrain telescope with an effective diameter of the primary mirror of 41.5 mm. The detector is a copy of PHEBUS/FUV on board the *BepiColombo* spacecraft (Yoshioka et al. 2012). A pixel scale is $0.^\circ033 \times 0.^\circ024$ per pixel and the effective FOV is $\sim 2^\circ \times 2^\circ$ on the sky. The imager can observe only the Lyα wavelength region of 122 ± 10 nm because of a bandpass filter.

Lyα images taken with the *PROCYON*/LAICA are reduced using IDL software. The FOV of each image included comet 67P/C–G as well as a field with a few stars used as a flat-field that was separated by 5° from the comet. The raw images are flat-fielded by the flat-field image on the assumption that the distribution of background interplanetary Lyα emission was uniform within the FOV of LAICA, which is valid for the comet far from the Sun in the sky. Flat-fielded images of the comet 67P/C–G are combined with alignment based on the positions of field stars (the motion of the comet during observations on each date can be neglected compared to the pixel scale). Thanks to the wide FOV of the LAICA instrument and positions of the 67P/C–G, the field stars were taken in the same frame with the comet. Thus, the resultant combined images for 67P/C–G are already normalized by the mean intensity of the interstellar region, and we subtracted the interstellar component from the normalized images. Mean and standard deviation of interplanetary Lyα emission in the background region are estimated from a region without both 67P/C–G and the field stars. Finally, we perform a flux calibration (a conversion from normalized count to intensity in Rayleigh units) by using the absolute Lyα intensities in the interplanetary background region on the observational dates. These absolute Lyα intensities of interplanetary background in a direction to the comet from the LAICA are referred to the archived observations by *SOHO*/SWAN[8] (352.9, 342.9, and 342.6 Rayleighs on UT 2015 September 7, 12, and 13, respectively). We consider the systematic error in absolute Lyα intensity in our observations as 30% originating in the flux calibration for the *SOHO*/SWAN's observations (Combi et al. 2014). Figure 1 (panels A, B, and C) shows the calibrated images of 67P/C–G of our observations.

3. RESULTS AND DISCUSSIONS

To estimate a water production rate from a single Lyα image, we use the two-dimensional axi-symmetric Direct

[8] http://swan.projet.latmos.ipsl.fr/

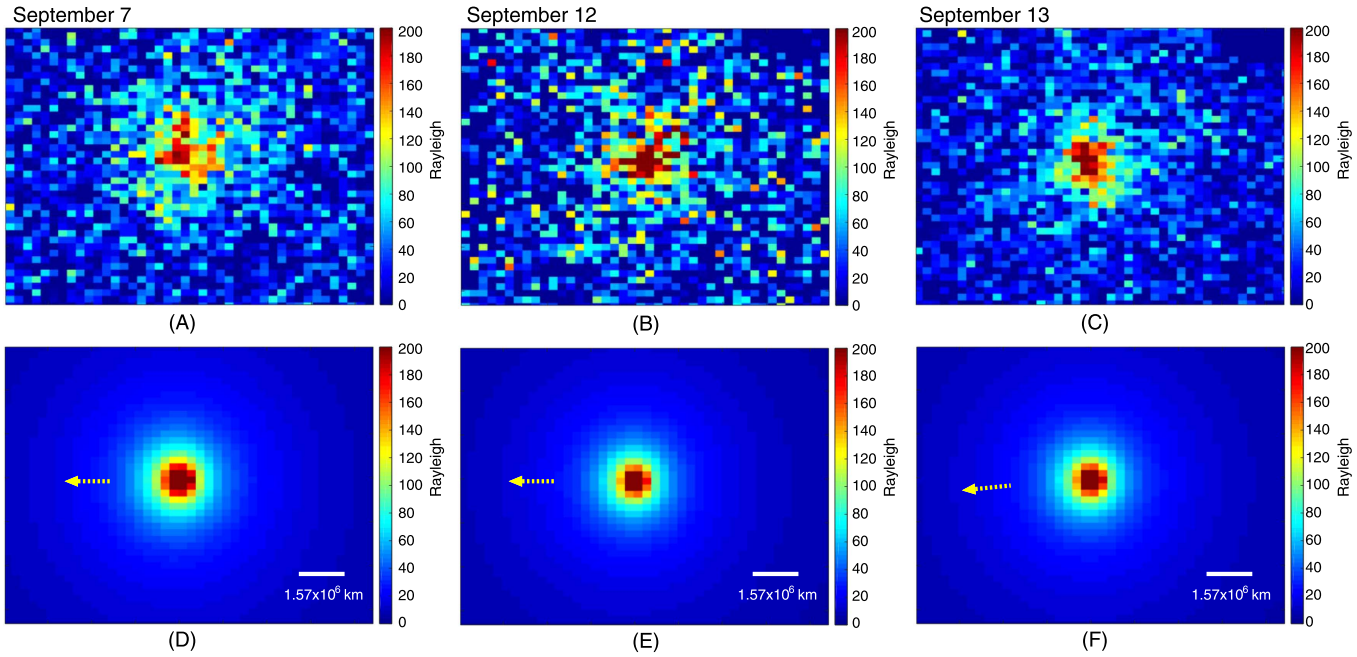

Figure 1. Trimmed reduced Lyα images of the comet 67P/C–G in Rayleigh units (upper three panels of A, B, and C) and reproduced images of hydrogen coma by the 2D axi-symmetric model from Tenishev et al. (2008) used similarly as in Crismani et al. (2015) (lower three panels of D, E, and F) on UT 2015 September 7 (left), 12 (center), and 13 (right), respectively. Yellow dotted arrows in the lower three panels indicate the Sun direction at the observations.

Table 2
Photochemical Reactions Considered by the 2D Axi-symmetric Model

Reactions	Wavelength (Å)	Product Velocities (Species) (km s^{-1})		Branching Ratio or Photodissociation Rate (10^{-6} s^{-1})[a]
Photochemical reactions of water				
$H_2O + h\nu \rightarrow H + OH$	1357–1860	17.5 (H)	1.05 (OH)	0.670
	1216	28.7 (H)	1.7 (OH)	0.176
	984–1357	28.6 (H)	1.5 (OH)	0.03
$H_2O + h\nu \rightarrow H_2 + O$	1357–1860	12 (H_2)	1.5 (O)	0.007
	1216	12 (H_2)	1.5 (O)	0.023
	984–1357	12 (H_2)	1.5 (O)	0.004
$H_2O + h\nu \rightarrow H + OH \rightarrow 2H + O$	1216	<5 (H)	<0.3 (O)	0.027
	984–1357	<5 (H)	<0.3 (O)	0.004
$H_2O + h\nu \rightarrow$ ionization product	<984	⋯	⋯	0.059
Photochemical reactions of OH radical				
OH ($A^2\Sigma^+$ $v' = 2$) + $h\nu \rightarrow$ H+O	2160	8 (H)	0.5 (O)	3.0–6.1
	2450	11 (H)	0.7 (O)	0.5
OH ($1^2\Sigma^-$) + $h\nu \rightarrow$ H + O	1400–1800	22–26 (H)	1.4–1.6 (O)	1.4
OH ($1^2\Delta$) + $h\nu \rightarrow$ H + O	1216	26.3 (H)	1.6 (O)	0.3
OH ($B^2\Sigma^+$) + $h\nu \rightarrow$ H + O	1216	17.1 (H)	1.1 (O)	0.05
OH ($2^2\Pi$–$3^2\Pi$) + $h\nu \rightarrow$ H + O	1216	26.4 (H)	1.6 (O)	0.05
OH ($D^2\Sigma^-$) + $h\nu \rightarrow$ H + O	<1200	22 (H)	1.4 (O)	<0.01

Note.
[a] Values of the rightmost column are the branching ratio and photodissociation rate for the reaction of water and OH radical, respectively.

Simulation Monte-Carlo (DSMC) model of atomic hydrogen coma using the Adaptive Mesh Particle Simulator code. This model was used to compute water production rates in a similar way from observations of comet C/2013 A1 (Siding Spring) with the Imaging Ultraviolet Spectrograph (IUVS) on board the *Mars Atmosphere and Volatile EvolutioN* (*MAVEN*) spacecraft (Crismani et al. 2015). In this model, hydrogen atoms are assumed to be produced by photodissociation of H_2O and OH, and have expected spatial and velocity distributions by considering radiation pressure of the Sun. As a result of the progressive dissociation of H_2O and OH in expanding gaseous coma, we can obtain an axi-symmetric profile of hydrogen coma. The photodissociation reactions used in this work are summarized in Table 2, which referred to Tables 2 and 3 of Tenishev et al. (2008). The coma model is optimized by χ^2 minimizing between the observations and synthesized hydrogen coma images in the range of 42 pixels by 42 pixels around the opt-center of the comet (Figure 1). We assumed the boundary conditions from Tenishev et al. (2008), which define the local surface temperature and gas flow depending on the

Table 3
Fitting Results of Power-law of Water Production Rates of 67P/C–G
(Fitting Function: Q_{H_2O} $(r_H) = Q_{H_2O}(1\ au) \times r_H^p$

Apparition	Q_{H_2O} at 1 au (s^{-1})	p
2015 (all)	$(5.82 \pm 0.61) \times 10^{28}$	-5.79 ± 0.38
2015 (pre-perihelion)	$(5.22 \pm 0.66) \times 10^{28}$	-6.00 ± 0.46
2015 (post-perihelion)	$(5.88 \pm 0.66) \times 10^{28}$	-5.22 ± 0.41
2009 (all)	$(2.9 \pm 1.5) \times 10^{28}$	-6.2 ± 2.2
2002 (all)	$(7 \pm 15) \times 10^{28}$	-6.7 ± 8.2
1996 (all)	$(7.6 \pm 9.7) \times 10^{28}$	-8.7 ± 4.6
1982 (all)	$(3.3 \pm 3.1) \times 10^{28}$	-5.4 ± 3.0

direction of the Sun. The model also considers both the radiation pressure to the hydrogen atoms as the anti-sunward force and the radiation of Lyα emission by the fluorescence excitation. We use the g-factor (fluorescence efficiency) of Lyα emission at the epoch of the observations of $1.37 \times 10^{-3}/r_H^2$ photons s^{-1} $atom^{-1}$ at r_H au in the middle of 2015 September. This parameter is used to convert a column density of hydrogen atoms into an emission rate of Lyα photons. The g-factor in the middle of 2015 September is estimated from the daily total solar Lyα fluxes from the LASP website[9] by considering the heliocentric distances and relative velocities of the comet relative to the Sun at the observations. We consider ~10% of systematic error for the g-factor, which is calculated based on the solar Lyα flux from the Upper Atmosphere Research Satellite (UARS) instrument (Woods et al. 2000). Note that the derived water production rates, by using the 2D axi-symmetric DSMC model from Tenishev et al. (2008), may be over-estimated up to ~10%, based on the typical chemical composition of 67P/C–G (Goesmann et al. 2015; Le Roy et al. 2015 and references therein) because of additional contribution to the observed hydrogen atoms by the photo-dissociation reactions of another species (such as CH_3OH, HCN, H_2S) in the coma.

The best-fit water production rates of 67/C–G are 1.46×10^{28}, 1.24×10^{28}, and 1.30×10^{28} molecules s^{-1} with reduced-χ^2 of 1.04, 1.04, and 1.38 on UT 2015 September 7, 12, and 13, respectively. For the model fitting, we fix the model parameters (e.g., scale lengths of related species, branching ratios for the photodissociation rate of related molecules), except for the water production rate. The random errors in the model fitting give about a 1% error of the water production rates for the worst case on September 13. Each resultant water production rate has a 32% water production rate. Total error includes a 1% uncertainty from a random error (i.e., from the fitting error of the model) and a 32% uncertainty as a systematic error caused by the uncertainties of flux calibration by *SOHO*/SWAN's observations of 30% as commented by Combi et al. (2014) and the uncertainty in g-factors of 10% as mentioned by Woods et al. (2000), respectively. Results are listed in Table 1.

First, we compare our results with the water gas production rates around the perihelion passage in 2015 estimated from in situ measurements by the *Rosetta* instruments. Our results are comparable to those based on the measurements by ROSINA DFMS with the 3D DSMC model (Fougere et al. 2016b). On the other hand, our results are smaller by a factor of ~2–3 compared to the results based on the measurements by ROSINA but with an empirical model (Hansen et al. 2016), while our results are larger by a factor of ~2–5 based on the measurements by VIRTIS-H with a 3D DSMC model (Bockelée-Morvan et al. 2016; Fougere et al. 2016b). Basically, our results are comparable to the estimated water gas production rates based on in situ measurements combined with coma models. Thus, the measurements of gas production rates based on the wide FOV observations of entire coma are necessary to judge the validity of coma models used for in situ observations by the *Rosetta* instruments.

By χ^2 minimizing with the Levenberg–Marquardt algorithm (Press et al. 1992), we fit the observed water production rates with a power-law function of heliocentric distance at <2.5 au (water ice fully sublimates within ~2.5 au from the Sun) among the past five apparitions. We use a fitting expression as $Q_{H_2O}(r_H) = Q_{H_2O}(1\ au) \times r_H^p$, where $Q_{H_2O}(1\ au)$ and p are the water production rate of the comet at 1 au from the Sun and the power-law index, respectively. We calculate the power-law fitting based on the data in both pre- and post-perihelion (Table 3 and Figure 2). Since no descriptions are found about errors for some results obtained from the measurements by *Rosetta* instruments, we do not include the errors for those results to estimate a power-law index. Water production rates of 67P/C–G in the 2015 apparition except our observations are referred to by Bieler et al. (2015b), Biver et al. (2015), Bockelée-Morvan et al. (2015), Fink et al. (2016), Fougere et al. (2016a), Fougere et al. (2016b), Gulkis et al. (2015), Lee et al. (2015), Migliorini et al. (2016), and Wedlund et al. (2016). We also refer the water production rates based on OH observations during the apparitions in 1982 and 1996 (A'Hearn et al. 1995; Crovisier et al. 2002; Feldman et al. 2004; Schleicher 2006), low-resolution spectroscopic observations of water by the *AKARI* satellite during the apparition in 2009 (Ootsubo et al. 2012), Lyα observations by *SOHO*/SWAN for the recent last three apparitions in 1996, 2002, and 2009 (Bertaux et al. 2014). As a result, we demonstrate that both $Q_{H_2O}(1\ au)$ and p of the all apparitions are within the error range. This result indicates no significant change in the slope of the water production rate within several apparitions, though the slope is probably related to dynamical age because 67P/C–G in the all apparitions shows a steeper slope of water production rates than typical Oort cloud comets (namely, dynamically younger comets). For the 2015 apparition, we demonstrated that slopes of pre- and post-perihelion within 2.5 au are -6.00 ± 0.46 and -5.22 ± 0.41, respectively (Table 3). These slopes are consistent with the slope derived by the all ROSINA DFMS data (–5.6; Fougere et al. 2016b), but inconsistent with the slopes by the ROSINA data with the empirical model (-5.10 ± 0.05 and -7.15 ± 0.08 for pre- and post-perihelion; Hansen et al. 2016). Schleicher (2006) reported the slopes for OH of -6.4 ± 2.1 and -5.4 ± 1.0 for pre- and post-perihelion, respectively, from their narrow-band photometric and imaging observations in the 1992 and 1996 apparitions. These results also indicate that the cometary activity in the 2015 apparition was comparable to those in the past apparitions since 1982. Note that large fitting errors are likely caused by the small number of samples (and therefore, we used the data of both pre- and post-perihelion). The minor problem with using pre- and post-perihelion data together is that a peak of water production rate was a few weeks after perihelion, not perihelion in the 2015 apparition (Bockelée-

[9] http://lasp.colorado.edu/lisird/lya/

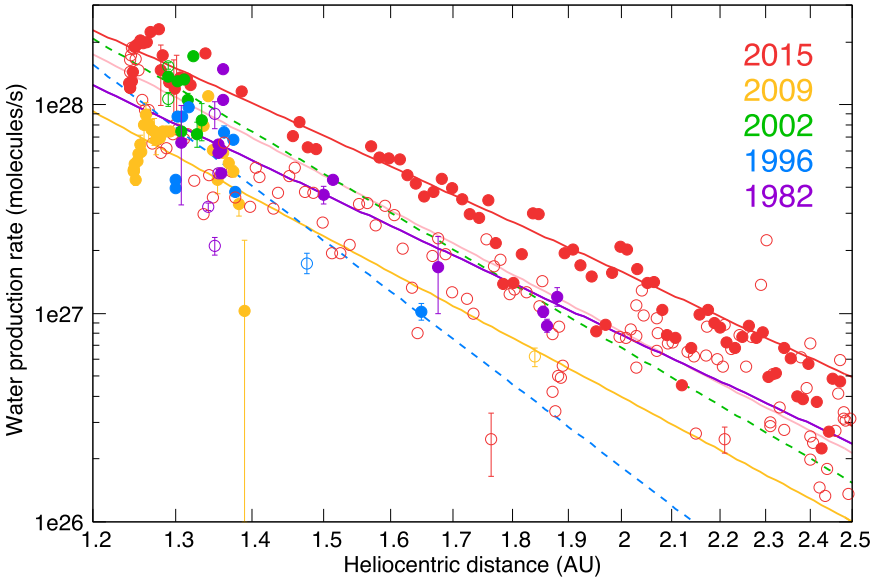

Figure 2. Water production rates of 67P/C–G for the five apparitions as a function of heliocentric distance. Colors of pink, red, orange, green, blue, and purple indicate the apparition in 2015 (pre-perihelion), 2015 (post-perihelion), 2009, 2002, 1996, and 1982, respectively. Open and closed circles indicate the observations of pre- and post-perihelion, respectively. Lines and dashed lines are results of power-law fitting of water production rates for each apparition by χ^2 minimizing. Note that dashed lines have large fitting errors (larger than 100% as relative error of either fitting parameters). References: water production rates of 67P/C–G in 2015 apparition were obtained from this work, *Rosetta*/COPS (Bieler et al. 2015b), *Rosetta*/ROSINA-DFMS (Fougere et al. 2016a, 2016b), *Rosetta*/MIRO (Biver et al. 2015, Gulkis et al. 2015, Lee et al. 2015), *Rosetta*/RPC-ICA (Wedlund et al. 2016), *Rosetta*/VIRTIS-H (Bockelée-Morvan et al. 2015), and *Rosetta*/VIRTIS-M (Fink et al. 2016; Migliorini et al. 2016). In the 2009 apparition, values were referred from *SOHO*/SWAN (Bertaux et al. 2014) and *AKARI*/IRC (Ootsubo et al. 2012). In the 2002, values were referred to in *SOHO*/SWAN (Bertaux et al. 2014). In the 1996 apparitions, values were referred to in *SOHO*/SWAN (Bertaux et al. 2014) and Schleicher (2006). In the 1982 apparition, values were referred to in A'Hearn et al. (1995), Crovisier et al. (2002), Feldman et al. (2004), and Schleicher (2006).

Morvan et al. 2016; Fougere et al. 2016b; Hansen et al. 2016). It is minor as long as this fits within the expected error range.

We check the relationship between the slopes and structures of cometary nuclei. Until now, there were four comets (19P/Borrelly by the Deep Space One in 2001, 9P/Tempel 1 by the Deep Impact mission in 2005, 81P/Wild 2 by the Stardust mission in 2006, and 103P/Hartley 2 by the *EPOXI* mission in 2010), which had taken detailed images of the nucleus surface prior to 67P/C–G. The derived slopes of water production rates of 9P/Tempel 1 and 103P/Hartley 2 were -4.0 ± 0.2 and -4.6 ± 0.1 (Meech et al. 2011) and -4.64 ± 0.22 and -3.99 ± 0.05 (Knight & Schleicher 2013) for pre- and post-perihelion, respectively. Those of 19P/Borrelly (-12.78 ± 0.43; A'Hearn et al. 1995) and 81P/Wild 2 (~–3; Mäkinen et al. 2001) were taken for only post-perihelion. 9P/Tempel 1 and 103P/Hartley 2 are classified as typical comets from the viewpoint of abundances of carbon-chain molecules like 67P/C–G, while 19P/Borrelly and 81P/Wild 2 are classified as carbon-chain-depleted comets (A'Hearn et al. 1995). As A'Hearn et al. (1995) pointed out, the slope of water production rates probably has a relation with dynamical age.

Bertaux (2015) reported that the total ejected masses per orbit of 67P/C–G for each of the last three apparitions were roughly estimated as $(1.13–2.55) \times 10^{10}$ kg in 1996, $(1.35–3.06) \times 10^{10}$ kg in 2002, and $(1.03–2.32) \times 10^{10}$ kg in 2009. These results correspond to a surface layer in 1.0 ± 0.5 m thickness and 0.1%–0.3% of total mass for the erosion rate and mass fraction lost in each orbit, respectively. Note that the thicknesses of lost material are estimated based on the assumption that materials were released from the entire surface area uniformly. We estimate the total ejected mass in the 2015 apparition based on the same method, and the derived total ejected mass is $(2.30–8.05) \times 10^{10}$ kg. The ejected mass is estimated by fitting the evolution of water production rates within 2.6 au and the same assumption as Bertaux (2015) for distances farther than 2.6 au. This mass-loss corresponds to 0.9–4.0 m for thickness and 0.19%–0.98% for mass-loss rate per orbit. These values are consistent with total mass loss of $(3.9–8.3) \times 10^{10}$ kg, mass-loss rate of 0.4%–0.6%, and thickness of 1.8–3.8 m during the 2015 apparition estimated from in situ measurements by the *Rosetta*/ROSINA (Hansen et al. 2016). As discussed above, 67P/C–G shows that the activity in the 2015 apparition was comparable to those in the past fourth apparitions at least. If this mass-loss rate per single apparition will be maintained in the future and the cometary nucleus will not be lost catastrophically by break up or disruption, the cometary nucleus of the 67P/C–G will disappear after a few thousand years.

Finally, we discuss active areas, S_A [m^2], and active area fractions, f_A [%], for our observations of 67P/C–G. We roughly estimate these parameters for our observations by using the averaged water production rate per unit area at 1 au depending on the angle θ between surface normal and the Sun direction, $Z = 0.69 \times 10^{22}$ molecules s^{-1} m^{-2}, shown in Table 2.1 of (Keller 1990, pp. 13–68). S_A and f_A are given by $S_A = Q_{H_2O}/Z(r_H)$ and $f_A = S_A/S_{67P}$, respectively, where $Z(r_H) = Z/r_H^2$, and surface area of 67P/C-G, S_{67P}, of 4.74×10^7 m^2 based on in situ measurements by the *Rosetta* spacecraft (Preusker et al. 2015). Averages of S_A and f_A for our observations are ~3.2×10^6 m^2 and ~6.8% at ~1.3 au from the Sun, respectively (see Table 1). As for the 2015 apparition, active area fractions become larger for closer distances from the

Sun (the average of active fractions of ∼1% at 3.5 au from the Sun; Gulkis et al. 2015 and Marschall et al. 2016). Filacchione et al. (2016) reported that the maximum fractions of water–ice abundances on the nucleus surface of 67P/C–G are about 1.2% and 4% for the areal and intimate sites with r_H of 3.4–2.9 au, respectively, by *Rosetta*/VIRTIS. These values are consistent with the results of ∼1% at 3.5 au, and the surface temperature of the nucleus at this distance (100–200 K; Gulkis et al. 2015) was comparable to sublimation temperature of water (∼150 K). At around the perihelion passage of 67P/C–G, both S_A and f_A in the 2015 apparition may be a little higher than the active area derived at 1.41 au in the 1982 apparition (1.3×10^6 m^2 for S_A and 2.72% for corresponding f_A; A'Hearn et al. 1995). Both S_A and f_A may become larger by approaching to the Sun. Snodgrass et al. (2013) reported the water active area on the surface of ∼1.4% based on the *R*-band light curve of 67P/C–G in the 1996, 2002, and 2009 apparition by fitting a thermophysical model and their model predicted an increase of the surface active area to ∼4% around perihelion. These results suggest that water vapor in the coma might evaporate from inner nucleus as well as from on the surface. This is consistent with the fact that most water likely sublimates from just below the dark refractory/organic surface layer most of the time, except for the few tiny areas of surface frost seen by *Rosetta*/VIRTIS (Filacchione et al. 2016). We also conclude that comet 67P/C–G is not a hyper-active comet like 103P/Hartley 2 (A'Hearn et al. 2011). Note that icy grains could also provide extra water gas in the coma. Until now, there has been no direct detection of icy grains in 67P/C–G, though there has been some possible evidence of sublimating icy grains (Gicquel et al. 2016). However, it seems like they would not contribute significantly to the total water production rate.

The authors sincerely thank the anonymous reviewer for constructive comments and suggestions that have helped us to improve our manuscript. The authors wish to thank Mr. S. Nakajima, Dr. J. Takisawa, Mr. S. Ikari, Mr. S. Ogura, Mr. Y. Kawabata, Dr. Y. Kawakatsu, and the *PROCYON* team for supporting our activities. We also acknowledge support from NASA Planetary Atmospheres grant NNX14AG84G to the University of Michigan. This research was supported by a Grant-in-Aid for Japan Society for the Promotion of Science (JSPS) Fellows, 15J10864 (Y. Shinnaka).

REFERENCES

A'Hearn, M. F., Belton, M. J. S., Delamere, W. A., et al. 2011, Sci, 332, 1396
A'Hearn, M. F., Millis, R. L., Schleicher, D. G., Osip, D. J., & Birch, P. V. 1995, Icar, 118, 223
Altwegg, K., Balsiger, H., Bar-Nun, A., et al. 2016, SciA, 2, e1600285
Bertaux, J. L. 2015, A&A, 583, A38
Bertaux, J. L., Combi, M. R., Quémerais, E., & Schmidt, W. 2014, P&SS, 91, 14
Bieler, A., Altwegg, K., Balsiger, H., et al. 2015a, Natur, 526, 678
Bieler, A., Altwegg, K., Balsiger, H., et al. 2015b, A&A, 583, A7
Biver, N., Hofstadter, M., Gulkis, S., et al. 2015, A&A, 583, A3
Bockelée-Morvan, D., Crovisier, J., Stephane, E., et al. 2016, MNRAS, 462, S170
Bockelée-Morvan, D., Debout, V., Erard, S., et al. 2015, A&A, 583, A6
Combi, M. R., Fougere, N., Mäkinen, J. T. T., et al. 2014, ApJL, 788, L7
Crismani, M. M. J., Schneider, N. M. S., Deighan, J. I., et al. 2015, GeoRL, 42, 8803
Crovisier, J., Colom, P., Gérard, E., Bockelée-Morvan, D., & Bourgois, G. 2002, A&A, 393, 1053
Feldman, P. D., A'Hearn, M. F., & Festou, M. C. 2004, in The New ROSETTA Targets, ed. L. Colangeli et al. (Dordrecht: Kluwer), 47
Filacchione, G., De Sanctis, M. C., Capaccioni, F., et al. 2016, Natur, 529, 368
Fink, U., Doose, L., Rinaldi, G., et al. 2016, Icar, 277, 78
Fougere, N., Altwegg, K., Berthelier, J. J., et al. 2016a, A&A, 588, A134
Fougere, N., Altwegg, K., Berthelier, J. J., et al. 2016b, MNRAS, 462, S156
Funase, R., Inamori, T., Ikari, S., et al. 2015, in 29th Annual AIAA/USU Conf. on Small Satellites, SSC15-V-5, 5
Gicquel, A., Vincent, J. B., Agarwal, J., et al. 2016, MNRAS, 462, S57
Goesmann, F., Rosenbauer, H., Bredehoft, J. H., et al. 2015, Sci, 349, aab0689
Gulkis, S., Allen, M., von Allmen, P., et al. 2015, Sci, 347, aaa0709
Hansen, K. C., Altwegg, K., Berthelier, J. J., et al. 2016, MNRAS, in press
Keller, H. U. 1990, in Physics and Chemistry of Comets, ed. W. F. Huebner (Berlin: Springer), 13
Knight, M. M., & Schleicher, D. G. 2013, Icar, 222, 691
Le Roy, L., Altwegg, K., & Balsiger, H. 2015, A&A, 583, A1
Lee, S., von Allmen, P., Allen, M., et al. 2015, A&A, 583, A5
Mäkinen, J. T. T., Silén, J., Schmidt, W., et al. 2001, Icar, 152, 268
Marschall, R., Su, C. C., Liao, Y., et al. 2016, A&A, 589, A90
Meech, K. J., Pittichová, J., Yang, B., et al. 2011, Icar, 213, 323
Migliorini, A., Piccioni, G., Capaccioni, F., et al. 2016, A&A, 589, A45
Ootsubo, T., Kawakita, H., Hamada, S., et al. 2012, ApJ, 752, 15
Press, W. H., Teukolsky, S. A., Vetterling, W. T., & Flannerty, B. P. 1992, Numerical Recipes in C: The Art of Scientific Computing (2nd ed.; New York: Cambridge Univ. Press)
Preusker, F., Scholten, F., Matz, K.-D., et al. 2015, A&A, 583, A33
Rubin, M., Altwegg, K., Balsiger, H., et al. 2015, Sci, 348, 232
Schleicher, D. G. 2006, Icar, 181, 442
Snodgrass, C., Tubiana, C., Bramich, D. M., et al. 2013, A&A, 557, A33
Tenishev, V., Combi, M., & Davidsson, B. 2008, ApJ, 685, 659
Wedlund, C. S., Kallio, E., Alho, M., et al. 2016, A&A, 587, A154
Woods, T. N., Tobiska, W. K., Rottman, G. J., & Worden, J. R. 2000, JGR, 105, 27195
Yoshioka, K., Murakami, G., Yoshikawa, I., et al. 2012, AdSpR, 49, 1265